Using models and satellite observations to evaluate the strength of snow albedo feedback

Christopher G. Fletcher,[1] Hongxu Zhao,[2] Paul J. Kushner,[3] and Richard Fernandes[4]

Received 1 March 2012; revised 9 May 2012; accepted 10 May 2012; published 15 June 2012.

[1] Snow albedo feedback (SAF) is important for global climate change, with strong regional impacts over northern continental areas. SAF calculated from the seasonal cycle is a good predictor of SAF in climate change among a suite of coupled climate models. A previous linear decomposition of the simulated total SAF (NET) found 80% was related to the albedo contrast of snow covered and snow-free land (SNC), and 20% was related to the temperature dependence of snow albedo (TEM). By contrast, recent work using snow cover and surface albedo derived from APP-x satellite observations found that TEM and SNC contributed almost equally to NET. In the present study, revised estimates of TEM and SNC for northern land areas are calculated for the period 1982–99 using a simplified and reproducible method for comparing SAF in models and observations. The observed NET is $-1.11\%\ K^{-1}$, of which 69% comes from SNC and 31% from TEM; the approximate additivity of SNC and TEM indicates that these two terms fully explain the total SAF. Regionally, the SNC term dominates equatorward of 65°N, while TEM dominates over the Arctic. The mean of 17 CMIP3 climate models shows NET is 7% larger than observed, caused primarily by a bias in TEM equatorward of 65°N. A newer model (NCAR CCSM4) with improved land surface and snow schemes reproduces observed values of NET and SNC closely. However, TEM in all models examined is 50–100% weaker than observed over the Arctic. There is a strong correlation between SAF in the seasonal cycle and SAF in climate change for all components, but the correlation is weakest for TEM. The TEM term also exhibits a much larger spread in the seasonal cycle than in climate change, which partially explains a discrepancy between previous published studies examining TEM.

Citation: Fletcher, C. G., H. Zhao, P. J. Kushner, and R. Fernandes (2012), Using models and satellite observations to evaluate the strength of snow albedo feedback, *J. Geophys. Res.*, *117*, D11117, doi:10.1029/2012JD017724.

1. Introduction

[2] *Qu and Hall* [2007] (henceforth QH07) showed that snow albedo feedback (SAF) processes exert a control over shortwave forcing in climate change, and that SAF strength varied threefold among the Coupled Model Intercomparison Project Phase 3 (CMIP3) coupled climate models, with no tendency toward a central value. They decomposed the total SAF into terms related to (*i*) the albedo contrast between snow covered and snow-free land at a given ambient temperature and (*ii*) the dependence of snow albedo on ambient temperature for a given snow fraction and albedo contrast. We denote the net albedo feedback, albedo contrast, and albedo-temperature terms NET, SNC, and TEM, and expect that NET = SNC + TEM (section 2). Among the CMIP3 models the contrast term SNC was the dominant term in both the mean and inter-model variation in SAF; that is, the TEM term was not as important for determining total SAF (QH07).

[3] *Hall and Qu* [2006] (henceforth HQ06) showed that, among the same ensemble of CMIP3 climate models, SAF in the winter-to-spring seasonal transition is a good predictor of SAF under climate change. Given that the SNC term is larger than the TEM term, the idea has emerged that models with a greater snow covered/snow-free albedo contrast show greater snow retreat in the winter-spring transition and a greater sensitivity of snow cover to greenhouse warming. The analogy between the climate response and the seasonal cycle suggests that if the seasonally based SAF can be accurately estimated from observations, then it should serve as an indicator of future SAF under climate change, and serve to constrain model responses to climate change.

[4] This report aims to update observational SAF estimates based on the winter-spring transition and to compare observed and model-simulated SAF as consistently as possible. Furthermore, because SAF can play a role in regional

[1]Department of Geography and Environmental Management, University of Waterloo, Waterloo, Ontario, Canada.
[2]Climate Research Division, Environment Canada, Toronto, Ontario, Canada.
[3]Department of Physics, University of Toronto, Toronto, Ontario, Canada.
[4]Canada Centre for Remote Sensing, Natural Resources Canada, Ottawa, Ontario, Canada.

Corresponding author: C. G. Fletcher, Department of Geography and Environmental Management, University of Waterloo, 200 University Ave. W, Waterloo, ON N2L 3G1, Canada. (chris.fletcher@uwaterloo.ca)

climate processes [*Fletcher et al.*, 2009; *Hall et al.*, 2008], this report also emphasizes the geographic distribution of parameters relevant to SAF. There has been a limited amount of work on this to date: *Hall et al.* [2008] produced observational estimates for the total SAF, NET, from two different satellite instruments, and found them to be inconsistent with each other but well within the spread of model estimates. *Flanner et al.* [2011] found that the CMIP3 models underestimate the annual mean net snow plus sea ice albedo feedback at the top of atmosphere (TOA). The starting point for the current study is *Fernandes et al.* [2009] (hereafter F09), who used Extended AVHRR Polar Pathfinder (APP-x) snow cover and albedo data [*Wang and Key*, 2005; *Zhao and Fernandes*, 2009] to estimate the geographic distribution of NET, SNC, and TEM. F09 directly calculated NET and SNC and then indirectly calculated TEM as a residual, via TEM = NET − SNC. In this first published observational estimate of the three terms, F09 found that TEM (which they refer to as "metamorphosis") and SNC were roughly equally important contributors to NET. This result suggests that the connections just described between snow-free/snow covered albedo contrast, the seasonal cycle, and climate responses might be simplistic.

[5] Thus, work comparing SAF in observations and models to this point leaves several questions unresolved: (*i*) Is the albedo-temperature effect TEM important in the SAF process in the seasonal cycle, and is it well captured in models? (*ii*) On a regional scale, how well, and with what uncertainty, do models capture SAF processes? And, (*iii*) can newly available satellite data products provide more accurate observational estimates of SAF? To address these questions, in this study we compute NET, TEM, and SNC in a robust and reproducible fashion from the APP-x satellite data, the CMIP3 model output, and output from a recently developed model of the CMIP5 class (the fourth generation NCAR climate model CCSM4 [*Gent et al.*, 2011]). This latter model's land surface scheme (now called CLM4) has undergone significant development and improvement in processes relevant to SAF [*Lawrence et al.*, 2012]. We produce hemispheric mean SAF estimates and spatially resolved SAF maps, with the intention of diagnosing model representation of this important climate process, which impacts global climate [*Budyko*, 1969; *Sellers*, 1969], continental hydrology [*Hall et al.*, 2008], and the atmospheric general circulation [*Fletcher et al.*, 2009].

2. Data and Methods

2.1. Theory

[6] Accounting for snow covered and snow-free surfaces, surface albedo (α_{sfc}) can be represented as

$$\alpha_{\mathrm{sfc}} = \alpha_{\mathrm{snow}} S + \alpha_{\mathrm{land}}(1 - S), \tag{1}$$

where α_{snow} is the snow albedo, S is the snow cover fraction, and α_{land} is the snow-free land albedo (F09, QH07). Assuming that S and α_{snow} are solely functions of surface temperature T, and that α_{land} is temperature-independent, we apply the chain rule of differentiation to (1) and find

$$\mathrm{NET}_{\mathrm{ideal}} = \mathrm{SNC}_{\mathrm{ideal}} + \mathrm{TEM}_{\mathrm{ideal}}, \tag{2}$$

where

$$\begin{aligned} \mathrm{NET}_{\mathrm{ideal}} &= \Delta\alpha_{\mathrm{sfc}}/\Delta T, \\ \mathrm{SNC}_{\mathrm{ideal}} &= (\alpha_{\mathrm{snow}} - \alpha_{\mathrm{land}})\Delta S/\Delta T, \end{aligned} \tag{3}$$

and,

$$\mathrm{TEM}_{\mathrm{ideal}} = S.\Delta\alpha_{\mathrm{snow}}/\Delta T,$$

[7] Equations (2) and (3) are essentially the same as equation 18 in QH07. The subscript "ideal" indicates that (2) and (3) arise from our idealized model of surface albedo (1). The term $\mathrm{NET}_{\mathrm{ideal}}$ represents the total SAF; $\mathrm{SNC}_{\mathrm{ideal}}$, (QH07's "snow cover component") represents how surface albedo varies when snow cover varies in the presence of a snow covered/snow-free surface albedo contrast; $\mathrm{TEM}_{\mathrm{ideal}}$, (QH07's "metamorphosis" component) represents changes to snow albedo with varying temperature, for fixed snow cover. The term $\mathrm{TEM}_{\mathrm{ideal}}$ potentially includes many processes, for example, metamorphosis of grain size in the snowpack, exposure of an underlying vegetated surface, and deposition of soot or debris onto the snow surface. In nature and in the models these processes often depend only indirectly on temperature. Using the idealized model requires these complex processes to be roughly represented in a single term. For this reason the idealized model should be checked for consistency as outlined below.

[8] Below we calculate independent estimates of the three terms $\mathrm{NET}_{\mathrm{ideal}}$, $\mathrm{SNC}_{\mathrm{ideal}}$, and $\mathrm{TEM}_{\mathrm{ideal}}$ and use the expected result of additivity from (2) to check the consistency of these estimates, and to avoid the practice of previous work (F09, QH07) in which additivity was used to constrain the calculation. Enforcing additivity introduces technical problems that will be described in the next subsection.

2.2. Computing Snow Albedo Feedback

[9] We diagnose SAF in terms of the change of 1982–1999 climatological monthly mean values of α_{sfc}, S and T during the transition from winter to spring. We consider three month-to-month transitions: one from March to April, a second from April to May, and a third from May to June. We average the results over all three transitions to produce a more robust picture of seasonally averaged SAF. Because we are interested in the impact of variations in α_{sfc} on the shortwave contribution to the surface energy budget, as in QH06 we weight all albedo quantities by the mean local climatological incoming shortwave radiation at the TOA (I) for each transition. For example, in the March to April transition the albedo fields are multiplied by March–April mean I normalized at each grid cell by the spatial average of I over the domain. This weighting therefore does not account for variations in surface insolation associated with clouds. We analyze only land areas poleward of 30°N with S greater than 0.1 in the first month of each transition. All SAF components are set to zero for land areas within the analysis domain where S is less than 0.1. Greenland is removed from all analyses, since not all models represent snow on ice sheets in the same way; snow lying on sea ice is also neglected. However, areas covered by smaller ice sheets (for example, those in the Canadian Archipelago) are retained, because models with lower spatial resolution tend to classify these areas as land.

Table 1. List of CMIP3 Models Used in This Study, and Their Number Index Used in Figures 1 and 4[a]

Number	CMIP3 Model Name	SNC	TEM
17	gfdl_cm2_0	72.0	23.6
16	miub_echo_g	45.3	50.0
15	gfdl_cm2_1	70.8	25.7
14	miroc3_2_medres	51.1	47.4
13	inmcm3_0	67.6	30.1
12	mpi_echam5	64.0	34.6
11	ncar_ccsm3_0	31.9	63.7
10	ukmo_hadcm3	79.7	15.8
9	ukmo_hadgem1	73.6	22.4
8	ipsl_cm4	57.1	40.3
7	cccma_cgcm3_1	64.7	33.6
6	cccma_cgcm3_1_t63	61.9	36.3
5	iap_fgoals1_0_g	27.4	70.8
4	csiro_mk3_0	84.4	11.1
3	giss_model_e_r	58.0	38.6
2	mri_cgcm2_3_2a	62.7	36.1
1	cnrm_cm3	54.1	44.6

[a]The models are ordered based on their values of NET from Figure 1. The third and fourth columns from the left show the relative contribution to NET, as a percentage, of the SNC and TEM terms, respectively. Further model details can be found online at: http://www-pcmdi.llnl.gov/ipcc/model_documentation/ipcc_model_documentation.php.

[10] We now summarize the procedure for estimating the idealized SAF terms for observations and models; further details are presented in Appendix A. Only climatological mean quantities serve as input into the calculations. The albedos α_{snow} and α_{land} are estimated from the surface albedo (α_{sfc}) and snow cover fraction (S) (F09). Land albedo α_{land} is estimated from typical post-snowmelt values of α_{sfc}, and is assumed constant in time, which is consistent with equations (1) and (2) (F09, QH07). Snow albedo α_{snow} is then estimated by inverting (1) using α_{land} and S. Then finite differences are used to compute estimates of the idealized SAF terms in (2) at each grid cell:

$$\begin{aligned} \mathrm{NET} &= \Delta\alpha_{\mathrm{sfc}}/\langle\Delta T\rangle, \\ \mathrm{SNC} &= (\overline{\alpha_{\mathrm{snow}}} - \alpha_{\mathrm{land}})\Delta S/\langle\Delta T\rangle, \end{aligned} \tag{4}$$

and,

$$\mathrm{TEM} = \bar{S}.\Delta\alpha_{\mathrm{snow}}/\langle\Delta T\rangle,$$

where deltas represent the change from one month to the next, overbars represent the time mean computed over the two months, and the angle brackets around $<\Delta T>$ indicate that the surface temperature change has been averaged over the entire analysis region poleward of 30°N. As mentioned, our results are then averaged over the three pairs of months. The same procedure is applied to models and observations.

[11] This method departs from F09 and QH07, where NET = SNC + TEM is used as a constraint to calculate the SAF terms. In F09, NET and SNC were calculated similarly to our current method, but TEM was calculated as the residual TEM = NET − SNC. The F09 calculation is thus additive but does not exploit the dependence of snow albedo on temperature that can be inferred via direct examination of the spatial and temporal variations in α_{snow}. The QH07 method uses NET = SNC + TEM as a constraint in a three equation inversion that solves simultaneously for α_{land}, α_{snow}, and a sensitivity function $F(T) = \Delta\alpha_{\mathrm{snow}}/<\Delta T>$. But using this method we found the results of QH07 difficult to reproduce because the linear inversion, and in particular the function $F(T)$, is sensitive to minor parameter changes. In summary, our current method provides an independent estimate of TEM (unlike F09), is simpler to implement and more robust than QH07 in models and observations, and provides additivity as a cross check.

2.3. Data Sources

[12] For diagnosing SAF in observations, α_{sfc} is taken from *Wang and Key* [2005], S from *Zhao and Fernandes* [2009], and T from the National Centers for Environmental Prediction – Department of Energy (NCEP-DoE) reanalysis [*Kanamitsu et al.*, 2002]. For diagnosing SAF in models, output for the period 1982–99 is taken from 17 models in the CMIP3 archive that completed the 20th Century historical forcings experiment (*20c3m*) (see Table 1 for a list of the models), as well as the historical 1-degree "all-forcings" CMIP5 simulation from the more recent NCAR CCSM4 model [*Gent et al.*, 2011]. An earlier version of the SAF analysis for CCSM4 was presented in *Lawrence et al.* [2012]; however, changes to our methods for computing SAF have resulted in slight differences to those results, and we also present several additional diagnostics here. We follow the methods of QH07 to estimate α_{sfc} as the ratio $Is_{\mathrm{u}}/Is_{\mathrm{d}}$, where Is_{u} (Is_{d}) is upwelling (downwelling) shortwave radiation at the surface, and to estimate S by converting from model output of snow mass per unit area (M) using a density threshold (d) of 60 kg m^{-2}:

$$\begin{aligned} S &= 1 | M >= d \\ S &= M/d | 0 < M < d \\ S &= 0 | M = 0. \end{aligned}$$

[13] This estimation of S is required since only around half of the models provided output of S directly. For those models with multiple realizations we use the ensemble mean from all available members (min = 2, max = 6).

[14] For all models and observations the SAF analysis is performed at the native output grid resolution; bilinear interpolation of the results to a common 2.5-degree latitude-longitude grid is performed prior to computing spatial averages. When computing spatial averages, the missing data mask of all fields is constrained to be the same as that in the observational S and α_{sfc} satellite data, which have the largest fraction of missing data as a result of the land-sea mask from the EASE grid projection of these data sets [*Zhao and Fernandes*, 2009].

[15] To facilitate a comparison with QH07, we also compute the SAF components in climate change using March–April–May (MAM) seasonal mean data. We define climate change in this study as the difference between the 30-year climatological average 2070–2099 (from the CMIP3 *sresa1b* scenario) minus the 30-year average 1900–1929. We elect to represent the future using data from the 21st Century, rather than the 22nd Century as QH07 did, because data from the new CCSM4 simulations were only available until 2100. However, we find (not shown) that the SAF results for the CMIP3 models are essentially the same when using

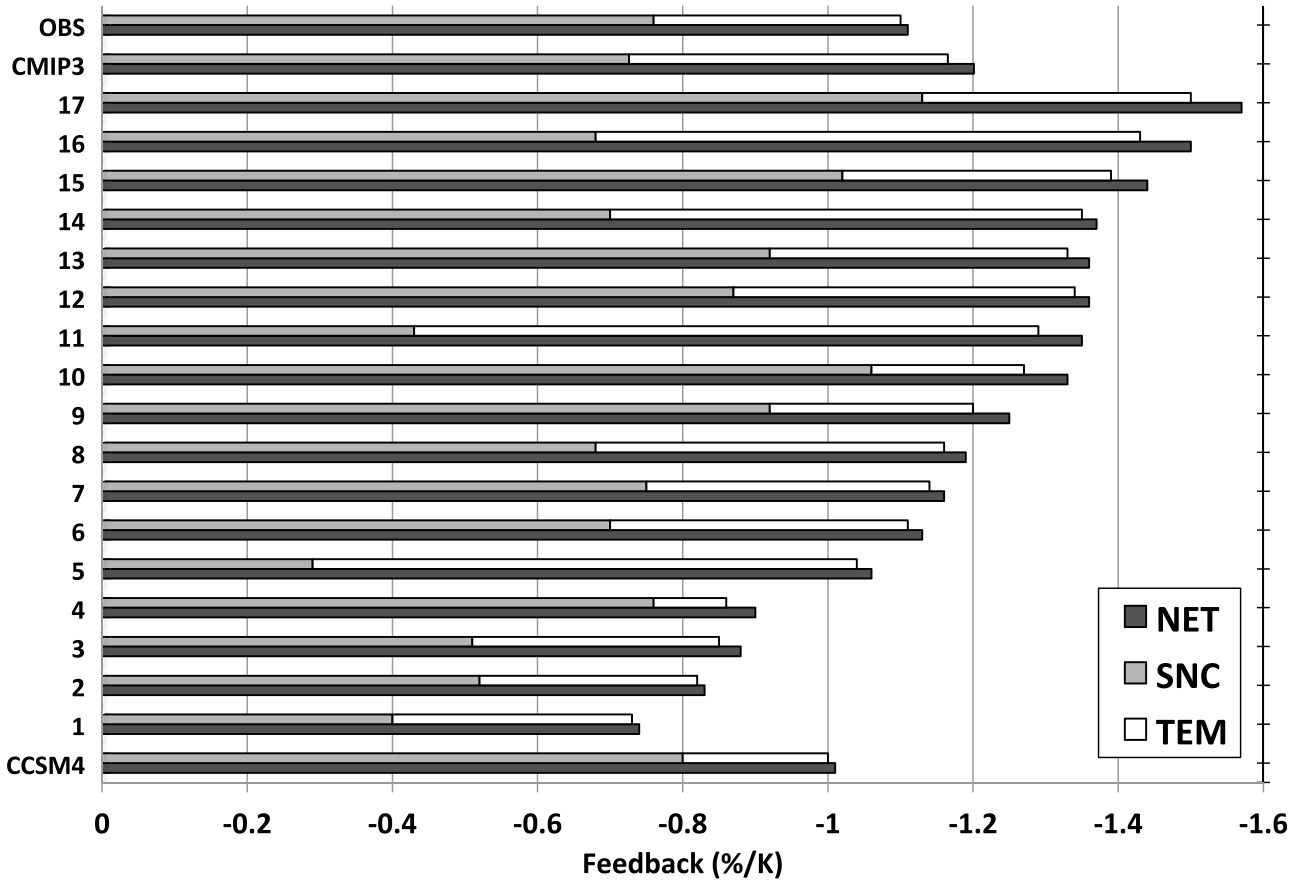

Figure 1. NH average MAMJ mean NET (darkest bars), SNC (mid gray bars) and TEM (white bars) components (units % K^{-1}) calculated from seasonal cycle data 1982–99. OBS are the observations, CMIP3 is the multimodel mean of the 17 CMIP3 models. The individual CMIP3 models are arranged in descending order of their NET term, and the CCSM4 model is shown at the bottom.

22nd Century data in place of 21st Century. All delta terms in the estimates in (4) are computed using MAM means. While annual means may be more relevant to global climate sensitivity than MAM means, in this and previous studies [*Fletcher et al.*, 2009; *Hall*, 2004; *Hall et al.*, 2008] the primary focus is on SAF as a driver of regional climate changes that peak in spring/summer. We tested the impact of extending the time period in the climate change calculations by one month to include June (to conform with the months used in the seasonal analysis), and found that the results are essentially unchanged (not shown).

[16] We find that the surface temperature perturbation over land areas poleward of 30°N associated with climate change has less than half the amplitude of the perturbation in the transition from winter to spring. In observations, the values of $<\Delta T>$ (see equation (4)) for the three transitions in the seasonal cycle are 7.77 K, 7.95 K and 6.97 K for MA, AM and MJ, respectively. The corresponding values for the 17-model CMIP3 mean are 9.03 K, 9.70 K and 8.74 K, respectively. By contrast, the CMIP3 mean value for climate change (2070–99 minus 1900–29) is 3.92 K. Thus, given that the temperature perturbations in the seasonal cycle and climate change have significantly different amplitudes, strong agreement between SAF components computed for these two timescales (shown for NET by *Hall and Qu*, [2006], and discussed here in section 3.3 for all components) would imply that the expressions in (4) are robust to large changes in $<\Delta T>$.

3. Results

3.1. Evaluation of NH Mean SAF Components

[17] In Figure 1 we present the spatially averaged NET, SNC and TEM diagnosed for the winter-spring seasonal transition; unless otherwise stated all values are in units of % K^{-1}, i.e., the percentage change in surface albedo per unit surface warming. The observations show a total feedback (NET) of −1.11 with 69% coming from the SNC term (−0.76) and 31% coming from the TEM term (−0.34). Since NET − (SNC + TEM) = −0.01, additivity is satisfied to within 1% for these three independently estimated terms. Thus, we conclude that the current method captures the principal physical processes contributing to the dependence of surface albedo on temperature in a self-consistent manner.

[18] The CMIP3 multimodel mean shows a total feedback (−1.20) that is close to observations; the residual is (−0.04) which falls within 4% of additivity (see Table 1 for the percentage contributions of SNC and TEM to NET in each model). The decomposition reveals that SNC (−0.73) is around 10% weaker than observations, but TEM (−0.44) is 30% larger, which causes the positive bias in total SAF. The newer model, CCSM4, has NET 10% weaker than observed,

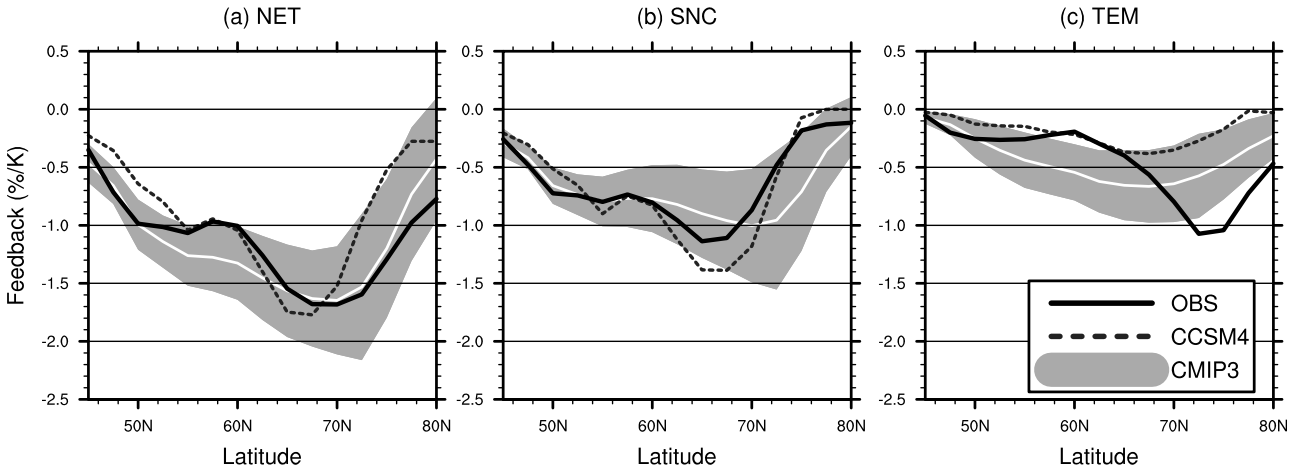

Figure 2. Zonal means of MAMJ mean (a) NET, (b) SNC and (c) TEM feedback components (units % K^{-1}) for OBS (solid black line), CCSM4 (dashed black line), the 17-model CMIP3 ensemble mean (white line) and standard deviation of the 17 CMIP3 models (gray envelope). The components are not evaluated equatorward of ~45°N, where *S* is generally less than 0.1.

which is traced to the TEM term having around two-thirds the amplitude of TEM in observations.

[19] Multiple sources of uncertainty affect the differences between the SAF components in models and observations. First, there is uncertainty resulting from the assumptions in the decomposition (2), which is manifest in the additivity of the SAF components; this explains the ~4% difference between NET and the sum of SNC and TEM in the CMIP3 mean. Second, there is uncertainty associated with imperfect model physics, which likely contributes to the ~30% bias in TEM relative to observations. However, there is also uncertainty in the observed NET, SNC, and TEM; from previous work [see, e.g., *Hall et al.* 2008] we expect that observational and estimation errors will lead to uncertainty on the order of 0.1 to 0.2% K^{-1} in these quantities, or 20% of NET. It is clear from Figure 1 that the majority of models fall outside this range of uncertainty expected from observations. The differences between observations and the CMIP3 mean are small compared to the wide spread among the models. This implies that even though the CMIP3 mean is close to observed it is not very representative of the behavior of most individual models, which was first made clear in QH07. We note there is a moderate anticorrelation between SNC and TEM in CMIP3 ($r = -0.46$). This is suggests there may be some cancellation of errors such that if SNC in a particular model is too weak, it is compensated by a stronger TEM, and vice versa. If SNC and TEM were both anomalously large (small), then the result would be NET that was much too strong (weak). The knock-on effect would be an unrealistic surface energy balance, and presumably an unrealistic winter-to-spring temperature transition.

[20] As mentioned in section 1, F09 and QH07 reported very different contributions to the total SAF from the TEM term. While our estimate of NET is consistent with these previous studies, we estimate a weaker TEM in observations than F09, and a stronger TEM with greater spread across the models than QH07. The comparisons are not straightforward but we have made some progress on this issue. First, we have discovered an error in the F09 results, related to a problem with insolation weighting, which leads to a significant reduction in their TEM value and provides estimates based on the residual method TEM = NET − SNC that are consistent with our observational estimate in Figure 1 (not shown). Second, the QH07 results estimate SAF in climate change, not in the seasonal cycle, and we will show in section 3.3 that TEM tends to be larger in the seasonal cycle than in climate change.

3.2. Spatial Variations in SAF Components

[21] Figure 2 plots the zonal mean SAF terms over 45°N–80°N (poleward of 80°N there are too few land grid cells for a robust calculation). In observations NET (Figure 2a) peaks around 70°N and from the decomposition it is shown that SNC (Figure 2b) dominates the total SAF at lower latitudes equatorward of 65°N, while TEM (Figure 2c) dominates at higher latitudes poleward of 65°N. We emphasize again that all of these quantities have been weighted by the local insolation at the top-of-atmosphere. The CMIP3 mean shows that NET is stronger than observed 50°N–60°N, which is caused by an almost factor of two bias in the TEM term (Figure 2c). By contrast, at higher latitudes NET in the CMIP3 mean is close to observed, which appears to be the result of compensating biases: SNC is stronger than observed, while TEM is much weaker than observed. Based on Figure 2c, we can also interpret the stronger than observed TEM in the CMIP3 hemispheric average (Figure 1) as resulting primarily from the positive bias at lower latitudes. The newer CCSM4 model lies generally within the spread of the CMIP3 models but, as shown in Figure 1, this model exhibits a very weak TEM term that contributes to the significant weak bias in NET at higher latitudes.

[22] The results from observations in Figure 2 suggest that distinct regimes may be operating poleward and equatorward of the Arctic Circle. The SNC term dominates in the temperate zone closer to the snow margin, while TEM dominates in the high Arctic and is representative of cold region hydrology. This makes sense physically, because SNC depends on snow cover melting to reveal land cover, and TEM depends on snow cover persisting long enough to undergo a change in its albedo. Since TEM dominates only

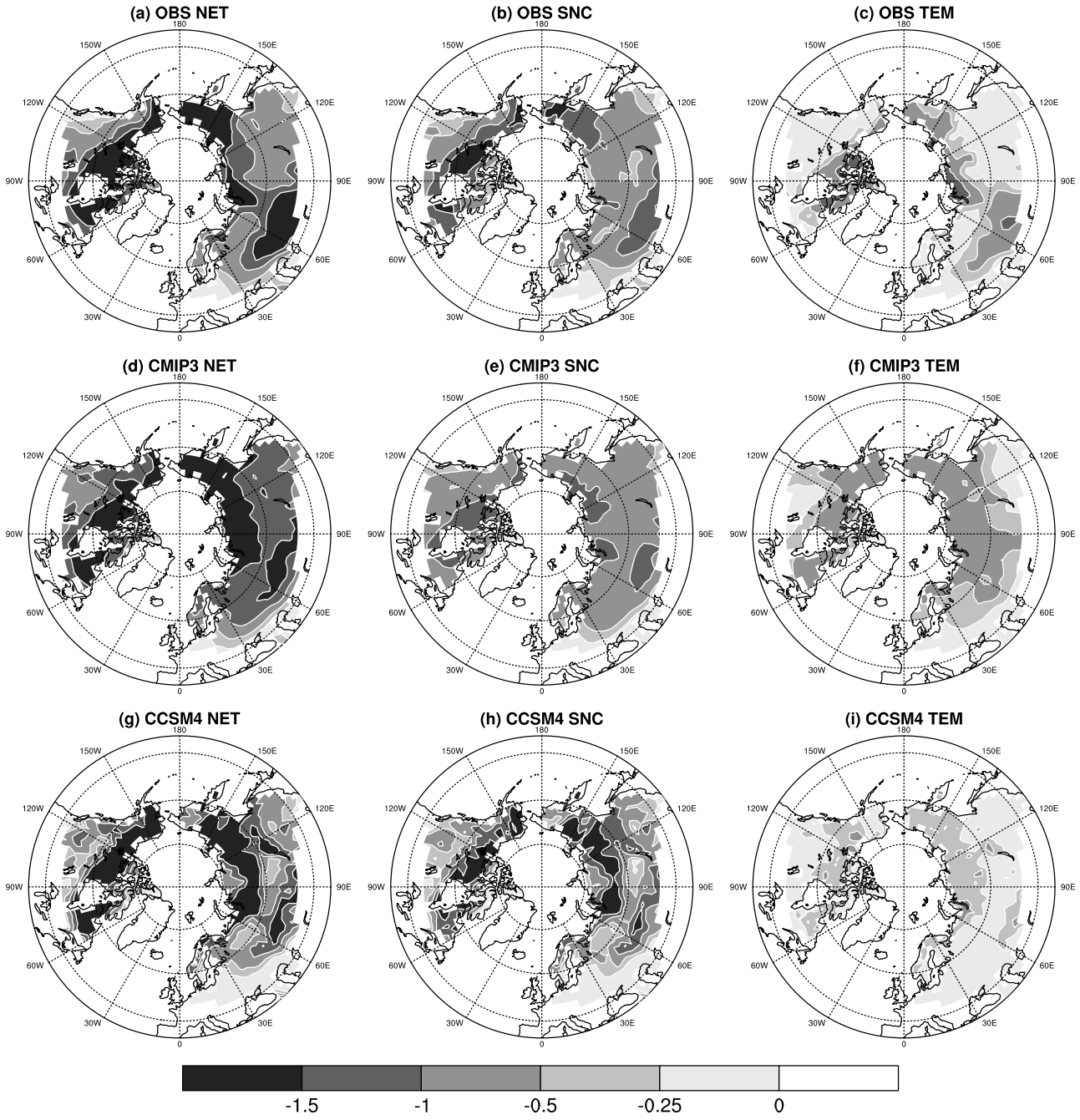

Figure 3. Northern Hemisphere MAMJ mean NET, SNC and TEM feedback components (units % K^{-1}) for OBS, CCSM4 and the 17-model ensemble mean of the CMIP3 simulations. Unshaded areas south of ~45°N are excluded from the analysis because $S < 0.1$ in all months.

over grid cells with persistent snow cover, our result offers an independent validation of QH07's method of training their function $F(T)$ over grid cells covered by pure snow, which were located predominantly over high northern regions. Overall, the models represent the lower latitude regime (SNC) well, but there are major differences between models and observations for the high Arctic (TEM) regime. The weaker than observed TEM at higher latitudes indicates a potential bias, common to the CMIP3 and CCSM4 models, in relation to changes in the Arctic hydrological cycle, which tend to be poorly simulated [*Arctic Monitoring and Assessment Programme*, 2005]. By contrast, the stronger than observed TEM at lower latitudes suggests that snow cover in the models is undergoing unrealistically large albedo variations there.

[23] The regional scale variations in SAF are displayed in Figure 3. In observations, NET (Figure 3a) peaks across northern Canada and northern Siberia, with a secondary peak over southwest Eurasia. The peak over North America is largely explained by the SNC term (Figure 3b), with little contribution from TEM (Figure 3c) except over far northern Canada and the Arctic Archipelago. Over Eurasia there is a

larger contribution to the total from TEM, particularly in north central and southwestern areas. This is in broad agreement with the results of F09, who showed a peak in TEM over north central Eurasia (computed as a residual for the April–May mean). The impact of these large localized values of TEM on the total SAF suggests that they could have a disproportionately large effect on the surface radiation balance, particularly in Arctic coastal regions where snow, land ice and sea ice are all in close proximity.

[24] The CMIP3 mean NET (Figure 3d) captures the observed spatial pattern but is stronger than observed across western North America, and across most of Eurasia. The spatial pattern of SNC (Figure 3e) is too weak over the Canadian tundra and northeastern Eurasia, while TEM (Figure 3f) has a more uniform distribution than observed and does not capture the localized maxima in Arctic coastal regions. Many of these differences stem from averaging the patterns from 17 models, which acts to smooth out spatial structure. The pattern for NET in CCSM4 (Figures 3g) more closely resemble observations; in particular, this model captures the peaks in far northern Siberia and North America, and the minimum over the Eurasian boreal forest at 60°N. However, the SNC term (Figure 3h) is somewhat stronger than observed, particularly over northern Eurasia, while in TEM (Figure 3i) the CCSM4 model broadly captures the observed spatial pattern, but with much weaker amplitude. F09 suggested that the observed peak in TEM over northern Siberia could be related to local impurities in the snowpack; however, we do not find evidence for highly elevated TEM in this region in CCSM4, which includes the effects of black carbon and mineral deposition on snow [*Lawrence et al.*, 2012].

3.3. Comparison of SAF in the Seasonal Cycle Versus Climate Change

[25] In this section we revisit the analogy proposed by *Hall and Qu* [2006] that SAF in the seasonal cycle can be used to better understand (and, ideally, to constrain) the strength and composition of SAF in climate change. Figure 4 compares the NH land average SAF components presented in Figure 1 for the seasonal cycle, with the SAF components computed from MAM seasonal means in climate change (see section 2.3 for details). As first presented by *Hall and Qu* [2006], our data show a strong relationship between NET in the seasonal cycle and climate change (Figure 4a), and we find a similar relationship for the SNC (Figure 4b) and TEM (Figure 4c) terms. For the NET and SNC terms, the CMIP3 models display a large spread around the observational value derived from the seasonal cycle, and the multimodel spread is slightly larger for climate change. The result for TEM is somewhat different; the multimodel mean and spread are both almost a factor of two larger in the seasonal cycle compared to in climate change. Thus, we can explain the differences in TEM between previous studies through the

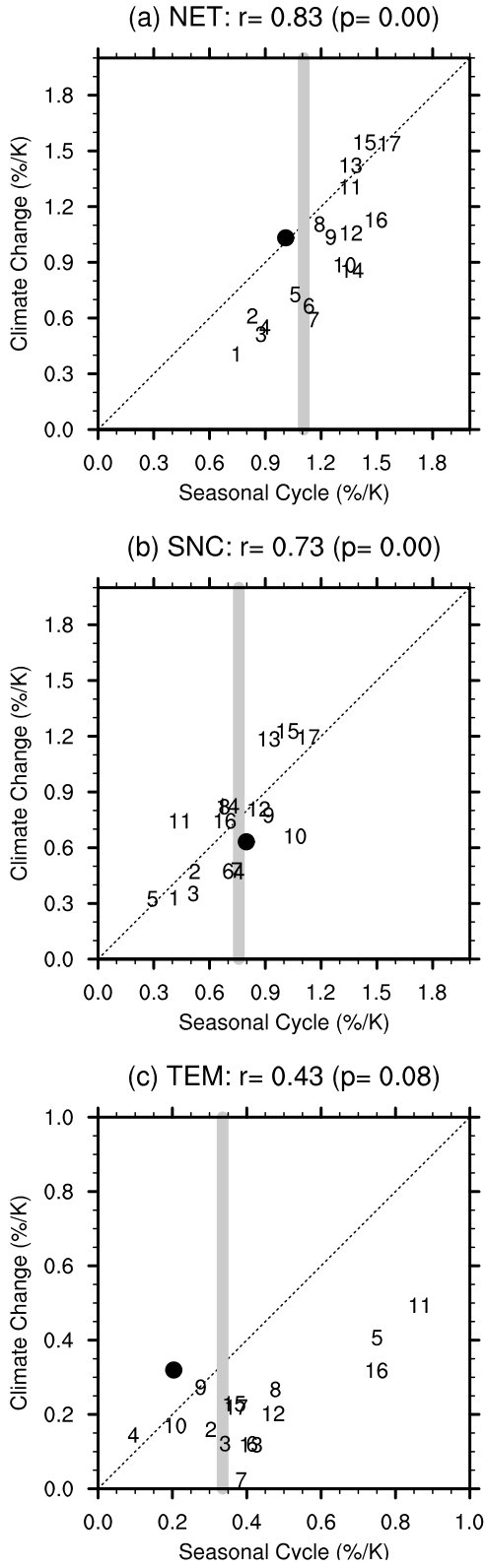

Figure 4. NH averaged values of (a) NET, (b) SNC and (c) TEM computed for the seasonal cycle versus climate change (all SAF values are multiplied by −1). The seasonal cycle data are averaged over MAMJ, while the climate change data are averaged over MAM. In each panel the 17 CMIP3 models are represented by the numbers listed in Table 1, CCSM4 is marked by the black dot, while the value for observations from the seasonal cycle is denoted by the thick gray vertical line. Pearson correlation values between the two variables are shown in the title of each panel, and the significance level (*p*-value) is indicated in brackets. The dashed diagonal line marks the 1:1 relation.

combination of a weaker TEM in climate change (QH07), and an error in insolation weighting (F09) (see section 3.1). The CCSM4 model lies close to observations, and to the 1:1 line, in NET and SNC, while CCSM4 is weaker than observed and further from the 1:1 line in TEM. In summary, the analogy of using the seasonal cycle to predict spring SAF in climate change holds strongly for SNC, and also for TEM with certain limitations, as demonstrated by the somewhat weaker correlation for this term ($r = 0.43$).

[26] Finally, QH07 found a strong correlation among the CMIP3 models between α_{snow} and NET in climate change, and a large range in α_{snow} from the models (0.28–0.59). They concluded from this result that the inter-model spread in SAF was mostly attributable to the spread in α_{snow}. Repeating this analysis using our data for NET and α_{snow} we also find a significant correlation ($r = 0.70$). Furthermore, we find a similar range for α_{snow} (0.32–0.54), which serves as a useful cross validation for our methods.

4. Discussion and Conclusions

4.1. Summary

[27] In this study we have produced a comparison of snow albedo feedback (SAF) in recently available satellite observations and a suite of climate models used in the Intergovernmental Panel on Climate Change (IPCC) fourth Assessment Report. We have extended existing theory and methods for diagnosing SAF in the present-day seasonal cycle, and devised a simplified method to decompose SAF into a component relating to the presence or absence of snow cover (SNC), and another component relating to the temperature dependence of snow albedo (TEM). Our findings suggest that 69% of the total observed feedback strength (−1.11% change in surface albedo per unit surface warming) is due to SNC, and 31% is due to TEM. In observations, SNC dominates the total SAF at latitudes equatorward of 65°N while TEM dominates over the Arctic, peaking in localized coastal regions. On average, the magnitude of SAF in the CMIP3 climate models is slightly larger than observed, due primarily to a positive bias in TEM at lower latitudes. The models also fail to capture the observed localized maxima in TEM over the Arctic. There is considerable spread of individual models around the multimodel mean in all components but, as found in climate change by QH07, the spread in NET is primarily explained by the spread in SNC. A newer climate model, CCSM4, reproduces the observed magnitude of NET to within 10%, and the spatial patterns of NET and SNC are well captured. However, SNC in this model is slightly stronger than observed, particularly over Eurasia, while TEM is much weaker than observed in all regions except around 60°N.

4.2. Discussion of Results

[28] Producing a robust comparison of SAF between models and observations has required certain subjective decisions in designing the methodology; for example, choosing to use a highly simplified model of surface albedo, and to use additivity among the SAF components as a consistency check instead of a requirement (see section 2.2). Despite the methodological differences between QH07, F09 and this study, we have been able to reproduce the primary results from these previous studies, and to bring to light an error that caused an artificial inflation of TEM in F09. Therefore, the primary contributions of this article are to reconcile previous results, and to present a simplified, reproducible methodology for computing SAF and its components from any data set that contains monthly climatologies of snow cover, surface temperature and surface albedo.

[29] In agreement with QH07, we have found a reduced role in climate change for the TEM term relative to SNC; however, we have also shown in Figure 4c that the magnitude of TEM is almost a factor of two larger in the seasonal cycle. This difference is perhaps unsurprising, since by construction the TEM term captures physical processes that are acting to modify the albedo of snow covered surfaces, and the relative contribution of individual processes depends on the timescale of interest. For example, changes in the rate of black carbon or mineral deposition on the snowpack from industrial emissions would be likely to occur much more slowly than the buildup of debris on snow (e.g., leaf litter, pine needles) during the winter-spring transition. Thus, while it is beyond the scope of this study, we believe there is important information that can be extracted by further decomposing the TEM term into its underlying physical processes. One simple method to achieve this would be to create a separate group of models with explicit representation of processes such as black carbon deposition, and to note whether TEM is any different in this group. Alternatively, process studies in climate simulations involving prescribed changes to the parameters governing snow albedo could be used to isolate individual processes [e.g., *Fischer et al.*, 2010], which in comparison with observations may contribute usefully to model development. This may require field campaigns to collect suitable observational data describing the strength of TEM over different land cover types.

[30] While *Hall and Qu* [2006] showed that the majority of CMIP3 models underestimated the observed NET, we find that 12/17 models have a larger NET than observed (Figure 1), suggesting that many models have unrealistically large snow-albedo sensitivity. An ongoing challenge to conclusive assessment is that, at this point, we do not have a good estimate for the observational uncertainty of SNC or TEM. This warrants a broader examination of SAF estimates from additional surface albedo data products from MODIS and GOES [*Govaerts and Lattanzio*, 2007] including computation of uncertainty using error propagation techniques [e.g., *Olson et al.*, 2006]. Impacts on SAF from changes in snow depth and snow density can also be compared in models and in observations, since appropriate field data products are available in some regions [e.g., *Dyer and Mote*, 2006].

Appendix A: Additional Methodological Details

A1. Spatial Averaging Procedure

[31] The spatial average of a quantity X, denoted by braces $\{\ldots\}$, is computed over a domain of grid cells R with surface area A [units m^2], with appropriate area weighting:

$$\{\mathrm{X}\} = 1/\Sigma[\mathrm{A}] \int_{i=\mathrm{R}}^{i=1} \mathrm{X}\, \mathrm{dA}.$$

A2. Calculation of α_{snow} and α_{land}

[32] This requires first computing max[α_{sfc}], which is the maximum monthly surface albedo on record in the February–June 1982–99 monthly climatologies (for the majority of grid cells the maximum albedo occurs in February or March):

$$\max[\alpha_{sfc}] = \max[\alpha_{sfc}(\mathrm{Feb}),\ \alpha_{sfc}(\mathrm{Mar}),\ \alpha_{sfc}(\mathrm{Apr}),\ \alpha_{sfc}(\mathrm{May}), \alpha_{sfc}(\mathrm{Jun})] \tag{A1}$$

[33] Second, α_{land} is defined as the mean α_{sfc} in the two months (mon1 and mon2) following snowmelt (where S first becomes less than 0.1).

$$\alpha_{land} = (\alpha_{sfc}|\mathrm{S} < 0.1_{mon1} + \alpha_{sfc}|\mathrm{S} < 0.1_{mon2})/2 \tag{A2}$$

[34] Next, α_{snow} is computed for all months March–June based on α_{sfc}, α_{land} and S:

$$\alpha_{snow} = [\alpha_{sfc} - ((1 - \mathrm{S})\alpha_{land})]/\mathrm{S} \tag{A3}$$

[35] As described in section 2.2, to mitigate against instability in (A3) we include only those grid cells where S > 0.1. We also take account of grid cells with small S by adding the following checks:

$$\begin{aligned} \alpha_{snow}(\mathrm{Mar}) &= \min[\alpha_{snow}(\mathrm{Mar}), \max[\alpha_{sfc}]] \\ \alpha_{snow}(\mathrm{Apr,\ May,\ Jun}) &= \min[\alpha_{snow}(\mathrm{Apr,\ May,\ Jun}), \\ &\quad \alpha_{snow}(\mathrm{Mar,\ Apr,\ May})] \end{aligned} \tag{A4}$$

[36] Thus α_{snow} in March cannot exceed the maximum surface albedo on record and α_{snow} in the subsequent months cannot exceed α_{snow} of the preceding month. Finally, for each month we ensure that $\alpha_{snow} = \max[\alpha_{snow}, \alpha_{land}]$; i.e., α_{snow} must always be greater than α_{land}. We also note that our method of calculating α_{snow} and α_{land} differs slightly from that in F09 because only monthly, rather than daily, α_{sfc} and S data were available as output from the models.

[37] **Acknowledgments.** We acknowledge the modeling groups, the Program for Climate Model Diagnosis and Intercomparison (PCMDI) and the WCRP's Working Group on Coupled Modeling (WGCM) for their roles in making available the WCRP CMIP3 multimodel data set. Support of this data set is provided by the Office of Science, U.S. Department of Energy. We thank David Lawrence (NCAR) for providing the CCSM4 data. This work was started while the investigators were supported by funds from the Canadian Cryosphere project of the International Polar Year. C.G.F. and P.J.K. are supported by grants from the Natural Sciences and Engineering Research Council, Canada. We thank Mark Flanner and two anonymous reviewers for their helpful comments.

References

Arctic Monitoring and Assessment Programme (2005), *Arctic Climate Impact Assessment*, Cambridge Univ. Press, Cambridge, U. K.

Budyko, M. I. (1969), The effect of solar radiation variations on the climate of the Earth, *Tellus*, *21*(5), 611–619, doi:10.1111/j.2153-3490.1969.tb00466.x.

Dyer, J. L., and T. L. Mote (2006), Spatial variability and trends in observed snow depth over North America, *Geophys. Res. Lett.*, *33*, L16503, doi:10.1029/2006GL027258.

Fernandes, R., H. Zhao, X. Wang, J. Key, X. Qu, and A. Hall (2009), Controls on Northern Hemisphere snow albedo feedback quantified using satellite Earth observations, *Geophys. Res. Lett.*, *36*, L21702, doi:10.1029/2009GL040057.

Fischer, E. M., D. M. Lawrence, and B. M. Sanderson (2010), Quantifying uncertainties in projections of extremes—A perturbed land surface parameter experiment, *Clim. Dyn.*, *37*(7–8), 1381–1398, doi:10.1007/s00382-010-0915-y.

Flanner, M. G., K. M. Shell, M. Barlage, D. K. Perovich, and M. A. Tschudi (2011), Radiative forcing and albedo feedback from the Northern Hemisphere cryosphere between 1979 and 2008, *Nat. Geosci.*, *4*(3), 151–155, doi:10.1038/ngeo1062.

Fletcher, C. G., P. J. Kushner, A. Hall, and X. Qu (2009), Circulation responses to snow albedo feedback in climate change, *Geophys. Res. Lett.*, *36*, L09702, doi:10.1029/2009GL038011.

Gent, P. R., et al. (2011), The Community Climate System Model Version 4, *J. Clim.*, *24*(19), 4973–4991, doi:10.1175/2011JCLI4083.1.

Govaerts, Y. M., and A. Lattanzio (2007), Retrieval error estimation of surface albedo derived from geostationary large band satellite observations: Application to Meteosat-2 and Meteosat-7 data, *J. Geophys. Res.*, *112*, D05102, doi:10.1029/2006JD007313.

Hall, A. (2004), The role of surface albedo feedback in climate, *J. Clim.*, *17*(7), 1550–1568, doi:10.1175/1520-0442(2004)017<1550:TROSAF>2.0.CO;2.

Hall, A., and X. Qu (2006), Using the current seasonal cycle to constrain snow albedo feedback in future climate change, *Geophys. Res. Lett.*, *33*, L03502, doi:10.1029/2005GL025127.

Hall, A., X. Qu, and J. D. Neelin (2008), Improving predictions of summer climate change in the United States, *Geophys. Res. Lett.*, *35*, L01702, doi:10.1029/2007GL032012.

Kanamitsu, M., W. Ebisuzaki, J. Woollen, S.-K. Yang, J. J. Hnilo, M. Fiorino, and G. L. Potter (2002), NCEP–DOE AMIP-II Reanalysis (R-2), *Bull. Am. Meteorol. Soc.*, *83*(11), 1631–1643, doi:10.1175/BAMS-83-11-1631.

Lawrence, D. M., K. W. Oleson, M. G. Flanner, C. G. Fletcher, P. J. Lawrence, S. Levis, S. C. Swenson, and G. B. Bonan (2012), The CCSM4 land simulation, 1850–2005: Assessment of surface climate and new capabilities, *J. Clim.*, *25*(7), 2240–2260, doi:10.1175/JCLI-D-11-00103.1.

Olson, W. S., et al. (2006), Precipitation and latent heating distributions from satellite passive microwave radiometry. Part I: Improved method and uncertainties, *J. Appl. Meteorol. Climatol.*, *45*(5), 702–720, doi:10.1175/JAM2369.1.

Qu, X., and A. Hall (2007), What controls the strength of snow-albedo feedback?, *J. Clim.*, *20*(15), 3971–3981, doi:10.1175/JCLI4186.1.

Sellers, W. D. (1969), A global climatic model based on the energy balance of the Earth-atmosphere system, *J. Appl. Meteorol.*, *8*(3), 392–400, doi:10.1175/1520-0450(1969)008<0392:AGCMBO>2.0.CO;2.

Wang, X., and J. R. Key (2005), Arctic surface, cloud, and radiation properties based on the AVHRR Polar Pathfinder dataset. Part I: Spatial and temporal characteristics, *J. Clim.*, *18*(14), 2558–2574, doi:10.1175/JCLI3438.1.

Zhao, H., and R. Fernandes (2009), Daily snow cover estimation from Advanced Very High Resolution Radiometer Polar Pathfinder data over Northern Hemisphere land surfaces during 1982–2004, *J. Geophys. Res.*, *114*, D05113, doi:10.1029/2008JD011272.